Pakistan Veterinary Journal

ISSN: 0253-8318 (PRINT), 2074-7764 (ONLINE)
DOI: 10.29261/pakvetj/2024.236

RESEARCH ARTICLE

Cilomilast, a PDE4 Inhibitor, Suppresses CD4$^+$ and CD8$^+$ T Cell Proliferation in the Thymus and Spleen of Rats: Mechanism of Glutathione Reduction

Arzu Gezer[1*], Nurcan Kılıç Baygutalp[2], Mustafa Cengiz[3], Bahri Gür[4*] and Mustafa Özkaraca[5]

[1*]Vocational School of Health Services, Atatürk University, Erzurum, Türkiye
[1*]Pharmaceutical Research and Development, Graduate School of Natural and Applied Sciences, Atatürk University, Erzurum/Türkiye
[2]Department of Biochemistry, Faculty of Pharmacy, Atatürk University, Erzurum, Türkiye
[3]Department of Elementary Education, Faculty of Education, Siirt University, Siirt, Türkiye
[4*]Department of Biochemistry, Faculty of Sciences and Arts, Iğdır University, Iğdır, Türkiye
[5]Department of Pathology, Faculty of Veterinary Medicine, Cumhuriyet University, Sivas, Türkiye
[*]Corresponding author: Arzu Gezer (PhD), arzu.gezer@atauni.edu.tr, Bahri Gür (PhD), bahri.gur@igdir.edu.tr

ARTICLE HISTORY (24-289)

Received: May 25, 2024
Revised: August 5, 2024
Accepted: August 5, 2024
Published online: August 27,2024

Key words:
Cilomilast
CD4$^+$, CD8$^+$
İn-silico modelling
Spleen
Thymus

ABSTRACT

Cilomilast is an oral phosphodiesterase-4 (PDE4) inhibitor recommended for treating COPD. However, its side effects and low therapeutic index remain an unresolved problem in clinical practice. This study aimed to evaluate the effects of cilomilast on the spleen and thymus tissues of rats. For experimental studies, 24 male *Sprague-Dawley* rats weighing 200-220g were randomly divided into three experimental groups: The procedures were repeated for 7 days for the control, sham, and cilomilast groups. Blood and tissue samples were collected from the rats under anesthesia on day 8 of the experiment for analysis. $p<0.05$ at a 95% confidence level was considered to indicate statistical significance. Severe tissue damage in the thymus and spleen was observed in the cilomilast group. In the thymus and spleen tissues of the control and sham groups, CD4$^+$ and CD8$^+$ cell immunopositivity were more intense, while the density of these cells was significantly reduced in the cilomilast group. In addition, glutathione (GSH) levels decreased, and nitric oxide levels increased in both tissues of the cilomilast group. However, *in-silico* results showed that the decrease in GSH levels is due to the enzymes γ-glutamylcysteine synthase and glutathione synthase, which act as catalysts in the two-step GSH biosynthesis mechanism. Suppression of the immune system targets both harmful and compensatory pathways so that both beneficial mechanisms and pathological changes can be blocked. To eliminate these cilomilast-induced side effects and enable more effective clinical application, it may be recommended to develop formulations such as lipid-based inhaled forms or nano-drug delivery systems including dendrimers, reverse micelle systems, polymeric or lipid-based carriers as an alternative to conventional application.

To Cite This Article: Gezer A, Baygutalp NK, Cengiz M, Gür B, Özkaraca M, 2024. Cilomilast, a PDE4 inhibitor, suppresses CD4$^+$ and CD8$^+$ T cell proliferation in the thymus and spleen of rats: mechanism of glutathione reduction. Pak Vet J, 44(3): 707-714. http://dx.doi.org/10.29261/pakvetj/2024.236

INTRODUCTION

Phosphodiesterases (PDEs) are a family of phosphohydrolase enzymes with 11 isoenzymes. PDEs have various functions depending on the organ in which they are located and are found in almost every tissue, including the lung, heart, brain, skeletal muscle, neonatal tissues, and partially immune and inflammatory cells. Four subtypes of PDE4 inhibitors, PDE4 (A, B, C, D), and about twenty isoforms/splicing variants are known. These isoforms, which are divided into long and short isoforms, can differ in their intracellular localization, three-dimensional structure, and cell-type expression. A PDE4 isoform fingerprint can be used to determine the potential efficacy of PDE4 inhibitors in different cell types and diseases. (Blauvelt *et al*., 2023). Besides, PDE4 primarily regulates epithelial and endothelial barrier stability, inflammatory responses, and mood or cognitive functions (Crocetti *et al*., 2022). PDE4 inhibitors have the potential to cause significant side effects outside the target

tissues of the respiratory tract. The PDE4 inhibitor has a limited dose and mechanical side effects, including headaches, vomiting, and diarrhea, due to its poor therapeutic index (Phillips, 2020).

Cilomilast, the second-generation PDE4 inhibitors, suppress the functions of inflammatory cells by reducing the production of cytokines that regulate the proliferation of T cells in respiratory diseases such as asthma and chronic obstructive pulmonary disease (COPD) due to their anti-inflammatory effects (Phillips 2020; Szczypka 2020). It shows greater efficacy and fewer side effects than first-generation inhibitors (Fan *et al*., 2024). Oral cilomilast is currently in phase III clinical trials for COPD treatment (Janjua *et al*., 2020). Studies have shown the inhibitory activity of PDE4 inhibitors on inflammatory and immune cells, including T cells (He *et al*., 2020). The spleen and thymus are lymphoid organs involved in immune responses to antigens (Lewis *et al*., 2019). Currently, no study in the literature has investigated the potential effects of cilomilast on thymus and spleen tissues in an experimental model.

The synthesis of glutathione (GSH) involves two enzymatic steps: the production of γGluCys and the catalysis of the association of γGluCys with Gly by glutathione synthase (GS). The γ-glutamylcysteine synthetase (GCL) consists of two subunits: the catalytic subunit (GCLC) and the modulator subunit (GCLM). Research indicates that knocking out the GCLC subunit results in embryonic lethality in mice, whereas knocking out the GCLM subunit permits survival.

This study was the first to investigate whether cilomilast has effects on the histopathology and biochemistry of thymus and spleen tissue in rats. In addition, the mechanism by which cilomilast affects the GSH was clarified *in-silico*.

MATERIALS AND METHODS

Chemicals: Cilomilast and dimethyl sulfoxide (DMSO) were acquired from Sigma Aldrich. Xylazine (Rompun®, Istanbul, Türkiye) and ketamine (Ketalar®, Istanbul, Türkiye) were sourced from Bayer and Pfizer, respectively.

Animals model: In the experimental studies, male rats were selected to avoid the effects of the menstrual cycle. 24 male *Sprague-Dawley* rats (200-220 g) were randomly assigned to one of three groups: the control group, the sham group, and the cilomilast group. Rats had ad libitum access to pellets and tap water in a room with a 12-hour light-dark cycle. All experimental procedures were approved by the Local Ethics Committee of Animal Experiments (28.12.2021-254). The details of the experimental groups (n=8) are as follows.

1. **Control group:** Rats were housed under standard conditions with no interventions.
2. **Sham group:** Rats received daily oral gavage of 0.2% DMSO solution (0.5 ml each day) (Flemming *et al*., 2014).
3. **Cilomilast group:** Rats were orally administered 3 mg/kg cilomilast (0.2% DMSO) (Strong, 2014).

These procedures were repeated for 7 days. On the 8th day, rats from all groups were deeply anesthetized with ketamine and xylazine for intracardiac blood sampling. Subsequently, the rats were euthanized by cervical dislocation. Thymus and spleen tissue samples were collected for histopathological, immunohistochemical analysis, and serum was obtained for biochemical analysis.

Histopathological examination: After sacrifice, the thymus and spleen samples were fixed, washed, and dehydrated. Following these steps, the tissues were infiltrated in xylol and then in paraffin, embedded in paraffin in metal blocks, and cut into hard blocks. 5 µm sections were prepared on microscope slides. Haematoxylin-eosin (H&E) staining was performed and the stained sections were semi quantitatively evaluated under light microscopy for necrotic and degenerative changes under a light microscope and graded as absent (-), mild (+), moderate (++), or severe (+++) (Gezer and Karadağ, 2023).

Immunohistochemical examination: Five-micron-thick sections on poly-lysine-thick slides were subjected to xylol and alcohol washes, followed by washing with PBS. Endogenous peroxidase was deactivated with 3% H_2O_2 for 10 minutes. Antigen retrieval was performed twice for 5 minutes at 500 W. After protein blocking, the slides were washed with PBS. Primary antibodies against $CD4^+$ (Santa Cruz, sc-19641) and $CD8^+$ (Santa Cruz, sc-1177) were incubated overnight at +4°C at a 1/100 dilution. The Large Volume Detection System: Anti-Polyvalent HRP (Thermo Fisher, TP-125-HL) was used as recommended. 3-Amino-9-ethylcarbazole served as the chromogen. After counterstaining with Mayer's haematoxylin, the slides were examined under a light microscope. Immunopositivity was quantified in 6 random areas (Sahin *et al*., 2022).

Biochemical analysis: Thymus and spleen tissues were stored at -80°C until analysis day. Tissues were ground with liquid nitrogen using a TissueLyser (Qiagen, Hilden, Germany). Then, 50 mg of tissue was added to 1 mL of PBS, followed by centrifugation. The protein content was determined using the Bradford method, which measures the absorbance shift of Coomassie Brilliant Blue G-250 dye in an acidic environment in the presence of proteins. GSH and NO levels in tissue homogenates were measured using ELISA kits (SunRed, Shanghai, China) per the manufacturer's instructions (GSH Ref no: 201-11-7122, Lot no: 202206; NO Ref no: 201-11-0704, Lot no: 202206). The absorbance values of the standard and the sample were read in an ELISA reader and the concentrations were calculated. The GSH and NO levels were reported as nmol/mg protein.

Molecular docking analysis: The molecular docking studies elucidated the mechanism of cilomilast's impact on GSH levels. The crystal structures of GCL (PDB ID: 6GMO) and GS (PDB ID: 1GLV) were obtained from the RCSB Protein Data Bank. Cilomilast structures were sourced from the PubChem database (Structure2D_CID_151170.sdf). PyRx and Discovery Studio 3.0 software were used for the analysis previously studies (Gür *et al*., 2023).

Table 1: Histopathological findings in the thymus and spleen.

	Control	Sham	Cilomilast
THYMUS			
Edema	0.33 ± 0.51[a]	0.33 ± 0.51[a]	1.83 ± 0.40[b]
Destruction of lymphoid cells	0.16 ± 0.51[a]	0.16 ± 0.51[a]	1.66 ± 0.51[b]
Degeneration in Hassal's corpuscle	0.00 ± 0.00[a]	0.16 ± 0.51[a]	1.83 ± 0.40[b]
SPLEEN			
Edema	0.16 ± 0.51[a]	0.16 ± 0.51[a]	1.66 ± 0.51[b]
Destruction of lymphoid cells	0.00 ± 0.00[a]	0.00 ± 0.00[a]	0.83 ± 0.40[b]

Note: [a,b]Different letters within the same row indicate statistically significant differences between groups. Significant differences ($p<0.05$) between the groups.

Interactions between GCL and substrates (glutamate and cysteine) were also examined. GCL catalyzes the rate-limiting step of GSH biosynthesis, forming a disulfide bond between Cys178 and Cys398 (Yang *et al*., 2019).

GS comprises three domains: the C-terminal, central, and N-terminal domains. GSH synthesis occurs in the cleft between the central and C-terminal domains. Analyses considered the GCLC and GCLM subunits for the Cilomilast@GCL complex and interactions between the central and C-terminal domain residues of GS and cilomilast for the cilomilast@GS complex.

Sample size calculation: The minimum number of rats required for the study was calculated using G*Power software (ver. 3.1.9.7). G Power inputs were one-way ANOVA test (two-sided), group number: 3, α (Type I error): 0.95, effect size: 0.25 (medium, Cohen's f), and 1-β (power): 0.975. G*Power software resulted in an output of 8 rats per group.

Statistical analysis: SPSS (version 25.0; IBM SPSS Inc., Chicago, IL, USA) was used. Normality was assessed with the Kolmogorov–Smirnov. Histopathological differences between groups were determined using the Kruskal–Wallis. The Mann–Whitney U test with Bonferroni correction was used for pairwise comparisons. Descriptive statistics (mean ± standard deviation) were employed. Independent samples t-tests and one-way ANOVA with post hoc Tukey tests were utilized for group comparisons. $p<0.05$ at the 95% confidence level was considered to indicate statistical significance.

RESULTS

Histopathological results: Normal histological features were found in the thymus and spleen tissues of the control and sham groups. In the cilomilast group, however, moderate histopathologic changes were found, particularly in the thymic medulla. These changes included edema, destruction of lymphoid cells, and degeneration of Hassal's corpus (Fig. 1A-C) (Table 1) ($p<0.001$ for all three parameters). On the other hand, in the spleen tissue of the cilomilast group, histopathological changes, including destruction of lymphoid cells and moderate edema, were observed mainly in the white pulp area. These changes included mild lymphoid cell destruction and moderate edema (Fig. 1D-F) (Table 1) ($p<0.001$ for both parameters).

Immunohistochemical results: Immunohistochemistry (IHC) of the thymus and spleen revealed decreased immunopositivity in the cilomilast group compared to the control and sham groups (Fig. 2A-L) ($p<0.05$). While the percentage of $CD4^+$ immunopositive cells was 45-49% in the control and sham groups, it decreased to 30% in the cilomilast group. Similarly, the percentage of $CD8^+$ immunopositive cells decreased in the cilomilast group (Table 2). These decreases were found to be statistically significant ($p<0.05$). On the contrary, in the spleen tissue, the percentage of both $CD4^+$ and $CD8^+$ immunopositive cells decreased in the cilomilast group while it was 40-44% in the control and sham groups (Table 2). These results were statistically significant ($p<0.05$).

Table 2: The number of $CD4^+$ and $CD8^+$ immunopositive cells (%) in the thymus and spleen.

	Control	Sham	Cilomilast
THYMUS			
$CD4^+$	47.00 ± 1.15[aA]	48.16 ± 1.37[Aa]	31.33 ± 1.20[Ba]
$CD8^+$	34.25 ± 2.14[aB]	32.41 ± 1.82[Ab]	21.62 ± 1.43[Bb]
SPLEEN			
$CD4^+$	43.40 ± 1.14[aA]	41.86 ± 1.23[Aa]	33.26 ± 0.45[Ba]
$CD8^+$	42.24 ± 1.06[aA]	40.71 ± 0.92[Aa]	31.82 ± 1.62[bA]

Note: [a,b]Different letters within the same row indicate statistically significant differences between groups. Show significant differences ($p<0.05$) between the groups. [A,B]Different letters within the same column indicate statistically significant differences between groups. Significant difference ($p<0.05$) between $CD4^+$ and $CD8^+$ (independent samples t-test).

Biochemical results: The findings indicated significant differences in GSH and NO levels between groups for both thymus and spleen tissues ($p<0.001$). It was revealed that significant differences between the control and cilomilast groups and between the sham and cilomilast groups for both thymus and spleen tissues (Table 3) ($p<0.05$).

Table 3: Biochemical markers of groups in thymus and spleen tissues (nmol/mg protein).

	Control	Sham	Cilomilast	*P*
THYMUS				
GSH	47.1 ± 4.4[a]	44.7 ± 3.8[b]	37.7 ± 3.2	<0,001
NO	5.9 ± 0.3[a]	7.0 ± 0.6[b]	17.6 ± 1.6	<0,001
SPLEEN				
GSH	51.1 ± 4.9[a]	55.0 ± 4.5[b]	27.7 ± 2.7	<0,001
NO	7.3 ± 0.6[a]	8.2 ± 0.8[b]	22.2 ± 3.3	<0,001

Note: [a, b]Show post-hoc Tukey test results of one-way ANOVA test. [a]Significant difference ($p<0.05$) between the control and cilomilast group, [b]Significant difference ($p<0.05$) between sham and cilomilast group.

***In-silico* results:** The GCL and GS binding sites were explored for cilomilast. These studies elucidated how cilomilast affects the activity of GCL and GS.

***In-silico* results of Cilomilast@GCL:** The results revealed the formation of the Cilomilast@GCL complex in both 2D and 3D (Fig. 3). As shown in Fig. 4c, cilomilast interacts with key active site residues of GCL, including Glu159, Pro160, Arg220, Met224, Trp296, and

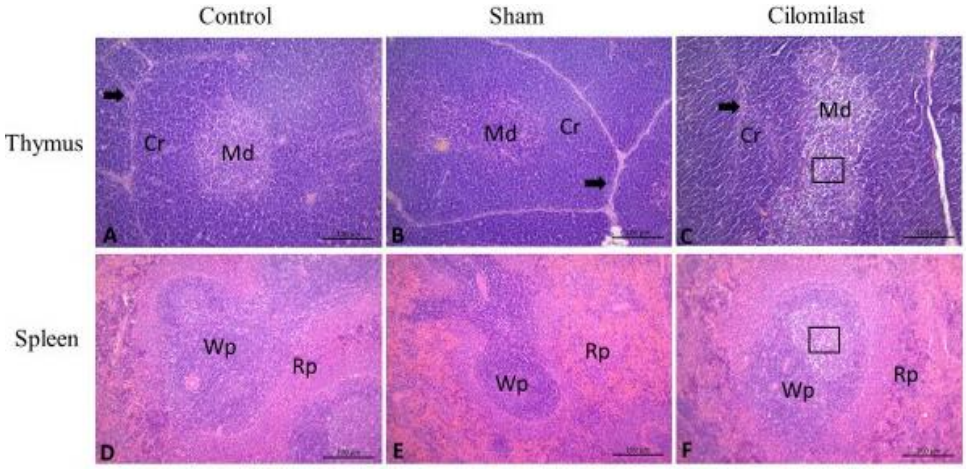

Fig. 1: Histopathological changes in thymus and spleen tissues. A. Control group; B. Sham group; C. Cilomilast group; D. Control group; E. Sham group; F. Cilomilast group. Cr: cortex, Md: medulla, Arrow: Hassall's corpuscle, □: edematous areas, Rp: red pulp, Wp: white pulp. H&E staining, scale bar 100 µm.

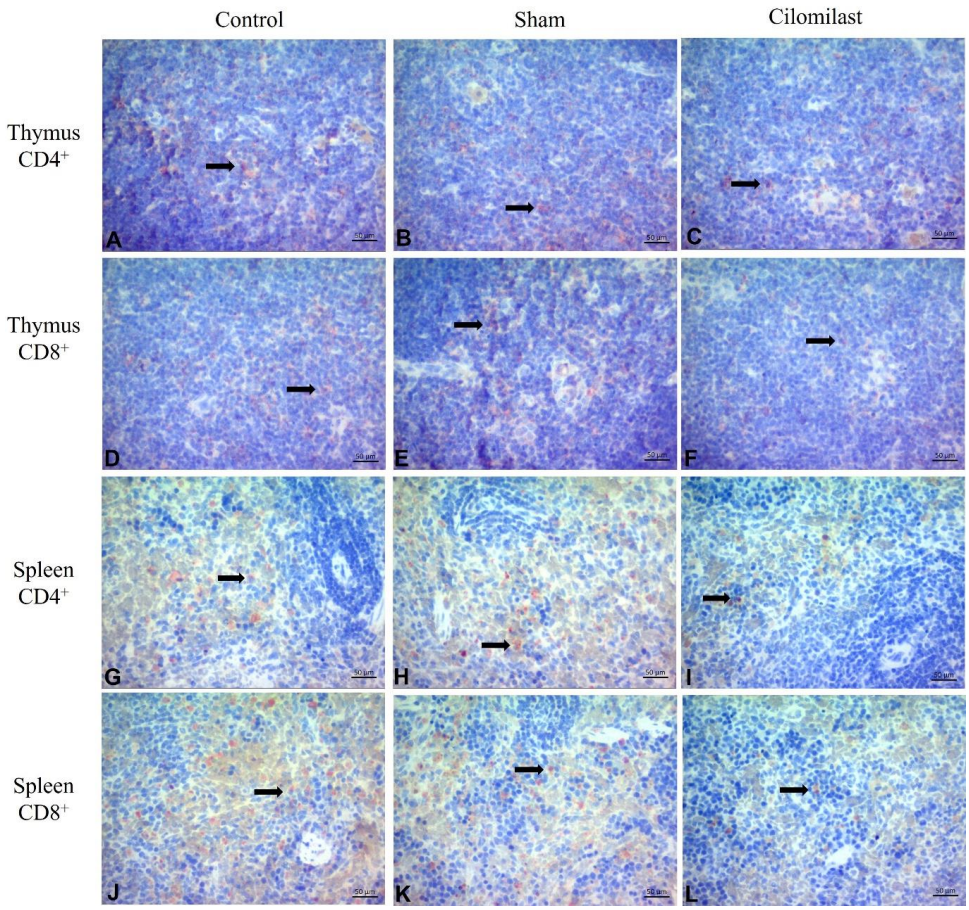

Fig. 2: Histopathological changes in thymus and spleen tissues. A. Control group, B. Sham group, C. Cilomilast group, D. Control group, E. Sham group, F. Cilomilast (arrows), G. Control group, H. Sham group, I. Cilomilast group, J. Control group, K. Sham group, L. Cilomilast group (arrows). IHC staining, scale bar 50 µm.

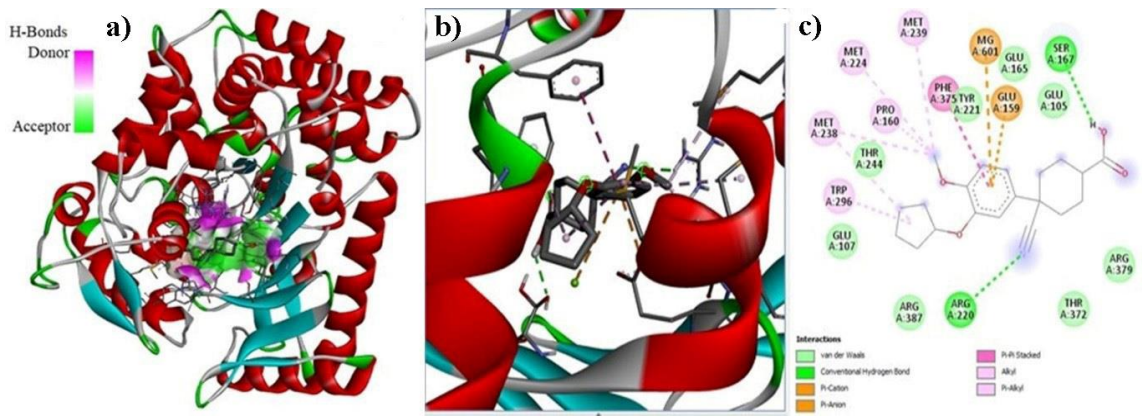

Fig. 3: (GLC). Demonstration of the Cilomilast@GCL complex resulting from the insertion of cilomilast into the active site of the GCL: **(a)** 3D general structure of Cilomilast@GCL complex showing H-Bonds interactions, **(b)** 3D zoomed ribbon image of interaction between amino acid residues of Cilomilast and GCL (Cilomilast stick structure), **(c)** 2D image of interaction types between cilomilast and amino acid residues of GCL.

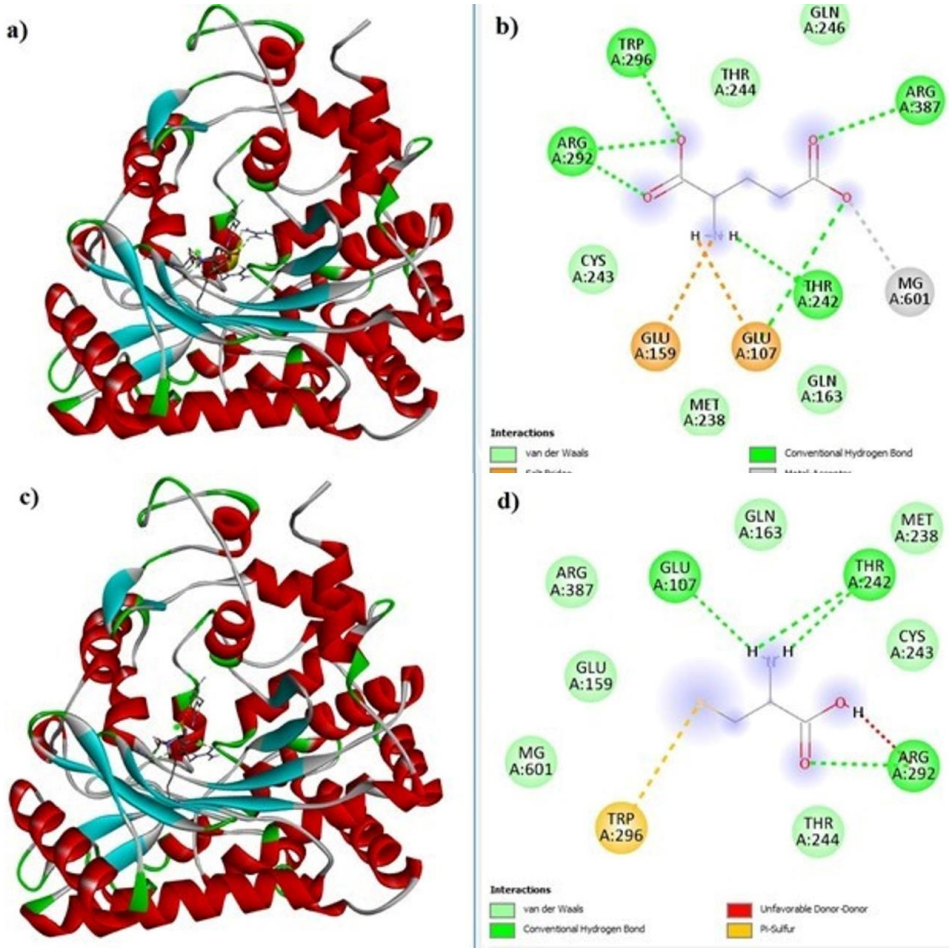

Fig. 4: (Glu and Cys GCL). Representation of the Glutamete@GCL and Cystein@GCL complexes formed by the insertion of glutamate and cysteine into the active site of GCL: **(a)** 3D general structure of the Glutamete@GCL complex (Glutamete stick structure), **(b)** Interaction between glutamete and amino acid residues of GCL **(c)** 3D general structure of Cystein@GCL complex (Cystein stick structure), **(d)** 2D zoomed ribbon image of interaction species between amino acid residues of Cystein and GCL.

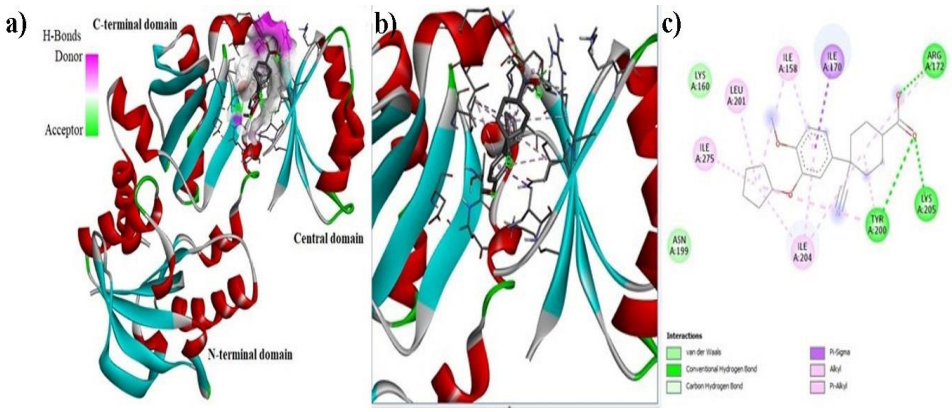

Fig. 5: (GS). Illustration of the Cilomilast@GS complex resulting from cilomilast insertion targeting the C-terminal, Central, and N-terminal domains of GS: **(a)** 3D overview showing the H-Bonds interactions of the Cilomilast@GCL complex and the placement of cilomilast in the C-terminal and Central domain cleft, **(b)** 3D zoomed ribbon image of interaction between amino acid residues of Cilomilast and GS (Cilomilast stick structure), **(c)** 2D image of interaction types between amino acid residues of Cilomilast and GS.

Graphical Abstract

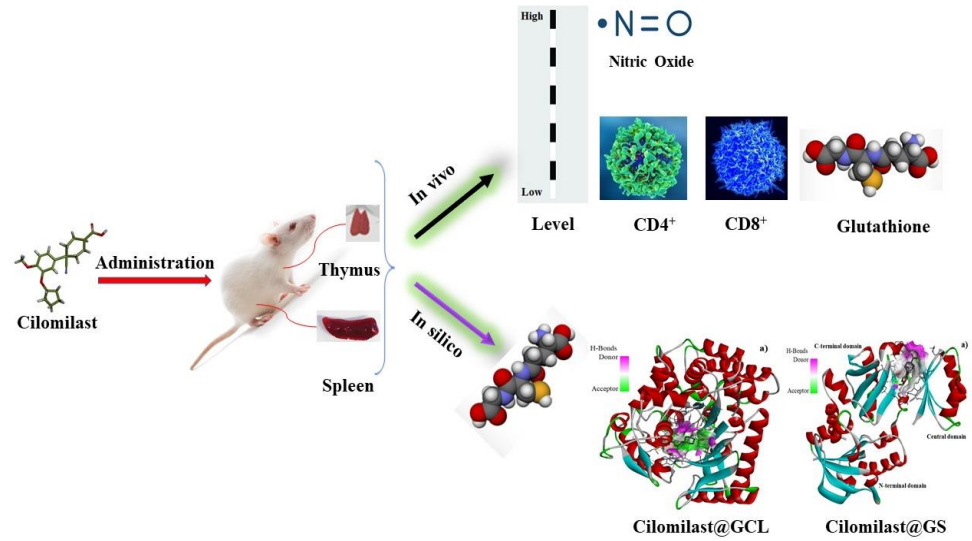

Phe375, alongside a pi-cation interaction with Mg2+. Additionally, the ligand exhibited van der Waals interactions with the active site residues. Notably, cilomilast did not disrupt the intramolecular disulfide bond between Cys178-Cys398 of GCL in the complex (ΔG: -7.8 kcal.mol-1).

***In-silico* results of Glutamate@GCL and Cysteine@GCL:** The results of Glutamate@GCL and Cysteine@GCL complex formation are illustrated in both 2D and 3D representations (Fig. 4). GCL interacts with specific amino acid residues, including Trp296, Glu107-159, Thr242, and Arg292-387, when glutamate serves as a substrate in the γGluCys dipeptide formation reaction. Additionally, glutamate was found to interact with the Mg2+ ion (Fig. 4a, 4b). Conversely, GCL interacts with Glu107, Thr242, Arg292, and Trp296 when cysteine acts as a substrate (Fig. 4c, 4d). The ΔG values of the Glutamate@GCL and Cysteine@GCL complexes were calculated as -5.7 kcal/mol and -4.6 kcal/mol, respectively.

***In-silico* results of cilomilast@GS:** The results of cilomilast@GS complex formation are depicted in both 2D and 3D representations, illustrating the binding of the cilomilast compound within the C-terminal, central, and N-terminal domains of this enzyme (Fig. 5). As shown in Fig. 5a, cilomilast docked within the cleft between the central domain and the C-terminal domain of the GS. Fig. 5c reveals cilomilast's interactions with specific residues, including Ile204 and Ile275 from the C-terminal domain, as well as Ile158, Ile170, Arg172, Tyr200, and Leu201 from the central domain of GS. The ΔG value was calculated to be 8.5 kcal.mol-1.

DISCUSSION

In this study, for the first time, we investigated the potential adverse effects of cilomilast on $CD4^+$ and $CD8^+$ cells in rats. Histopathological analysis revealed that cilomilast caused severe damage to thymus and spleen tissue as well as a decrease in the immunopositivity of $CD4^+$ and $CD8^+$ cells. The findings of this study are consistent with the literature. For example, one study showed a significant decrease in subepithelial $CD8^+$ lymphocytes in bronchial biopsies of COPD patients following cilomilast treatment (Kim *et al*., 2021). Similarly, cilomilast treatment decreased the amounts of $CD8^+$ T lymphocytes and $CD68^+$ macrophages in COPD patients (Nguyen *et al*., 2023). Given that the inflammatory mechanism of COPD is primarily associated with elevated levels of neutrophils, macrophages, and T lymphocytes, these findings hold considerable importance.

Oxidative stress, another critical mechanism influencing the development and outcome of COPD, induces inflammation by activating signalling molecules within inflammatory pathways (Barnes, 2020). Inflammation triggers oxidative stress by producing different reactive oxygen species (ROS)/reactive nitrogen species (RNS) through inflammatory cells located at the site of inflammation (Gür *et al*., 2020; Can *et al*., 2022). Furthermore, radicals increase the synthesis of various inflammatory cytokines/chemokines and enzymes. This association between oxidative stress and inflammation leads to the onset and progression of various pathological conditions (Cengiz *et al*., 2023). This interaction may be more significant in COPD, where there is a reduction in the body's normal antioxidant capacity in response to increased oxidative stress. Promising studies on oxidative stress-based therapeutics for COPD are ongoing (Barnes, 2020). Increased oxidative stress could exacerbate the prognosis of COPD patients. Both residential and inflammatory cells in the airways produce NO (Xu *et al*., 2020). Fractional exhaled NO is considered a useful biomarker for early COPD diagnosis and severity assessment (Liu *et al*., 2020). Serum NO levels were found to be lower in COPD patients compared to healthy people (Aydin *et al*., 2017), as well as in rats (Zhang *et al*., 2022). The level of GSH, an endogenous antioxidant system marker, has been reported to be lower in experimental models (Ju *et al*., 2022; Gür *et al*., 2023) and in COPD patients (Ismail *et al*., 2015). Xenobiotics are known to increase free radical formation (Donato and Tolosa, 2021). The presented results indicate that cilomilast negatively affects the antioxidant system and stimulates the oxidant system, as evidenced by the reduction in GSH and increase in NO levels in both tissues. We cannot exactly guess the possible mechanisms of GSH and NO, since there is no available study with the same protocol in the literature. Decreased tissue GSH levels and increased NO levels (similar to presented results) were determined in an experimental spleen toxicity model (Khan *et al*., 2014), and in an experimental oxidative aging model (Liu *et al.*, 2019). One of the possible mechanisms of NO is inducing apoptosis in spleen lymphocytes from MRL/lpr mice (Xu *et al*., 2020). An experimental toxicity study induced by deltamethrin has reported similar GSH and NO results in both thymus cells and spleen cells. A possible underlying mechanism is reported as apoptosis activated by caspase 3 (Kumar *et al.*, 2023). In line with the literature, the results of this current study showed that cilomilast administration decreased GSH levels and increased NO levels in both tissues, indicating a negative effect on the antioxidant system. It can be suggested that the administered dose of cilomilast (3 mg/kg) aggravated oxidative stress in COPD patients and may worsen the clinical picture since it is well-known that the relationship between oxidative stress and inflammation plays a role in the induction and progression of COPD.

In-silico results revealed that cilomilast interacts with the catalytic subunit of GCLC. These interactions include a π-anion with Glu159, alkyl with Pro160 and Met224, two conventional hydrogen bonds with Arg220, a π-alkyl with Trp296, and π-π stacked with Phe375. Additionally, cilomilast also exhibited a π-cation interaction with Mg2+, which is crucial for catalytic activity in GCL. Based on these findings, cilomilast inhibited GCL, which is essential for the first step of GSH synthesis.

From another perspective, in the formation of γGluCys, glutamate as a substrate should interact with Mg2+ along with the Trp296, Glu107-159, Thr242, and

Arg292-387 residues of GCL. However, in the presence of cilomilast, Trp296, Glu159, and Mg2+ of GCL are obstructed by cilomilast, leading to a decrease in the catalytic effect of GCL on glutamate substrates due to van der Waals. In contrast, in the γGluCys formation reaction, GCL is expected to interact with Glu107, Thr242, Arg292, and Trp296 because of its interaction with cysteine. However, the inhibition of Glu107, Trp296, and Mg2+ by cilomilast and the formation of van der Waals interactions indicate that cilomilast inhibits GCL catalysis toward the formation of γGluCys. These results are consistent with previous studies demonstrating that GCL catalyzes the formation of γGluCys (Luo *et al*., 2021).

The evaluated inhibition mechanism of cilomilast on glycine addition to γGluCys, cilomilast was bound to the cleft between the central domain of GS and the C-terminal domain (Fig. 7). That is, cilomilast blocked the area where the ATP molecule is located and inhibited GS by interacting with GS residues through conventional hydrogen bonds and alkyl and π-alkyl interactions in this region, thereby creating a steric barrier to glycine. These results indicate that cilomilast inhibits GS, which catalyses the second step of GSH biosynthesis, leading to a reduced yield of mature GSH (Montrose and Galluzzi, 2019). Presented *in-silico* results indicate that the observed biochemical decrease in GSH levels is due to reductions in both GCL and GS activities.

Conclusions: The findings of the current study are expected to significantly contribute to the literature on the adverse effects of cilomilast on the immune system, as evidenced by the reduction in $CD4^+$ and $CD8^+$ cells in the thymus and spleen tissues. In addition to the damage observed in these tissues in the cilomilast group, significant alterations in GSH and NO levels further indicate tissue damage. It can be concluded that integrating antioxidant therapy into standard treatment should be evaluated by clinicians to reduce the oxidative damage and pro-inflammatory effects caused by COPD drugs. Developing potential standardized formulations such as nanocarriers and conducting detailed analyses of cilomilast for clinical use should be considered. Furthermore, broader studies involving various tissue samples (sputum, bronchial biopsies, and bronchoalveolar lavage) are warranted to assess the toxic effects of cilomilast on immune and antioxidant systems.

Funding: This study protocol was reviewed and approved by the Scientific Research Commission of the Atatürk University, approval number [TAB-2022-10151].

Credit author statement: We confirm that this work is original and has not been published elsewhere, nor it is currently under consideration for publication elsewhere.

Conflict of interest statement: The authors declare no conflict of interest.

Authors contributions: AG: Corresponding Author, Methodology, Investigation, Data Curation, Review, Experimental studies. NKB: Statistical analyses, Visualization, Investigation, Data Curation, Conceptualization, Methodology, Formal analysis. MC: Data Curation, Conceptualization, Methodology, Formal analysis. BG: Corresponding Author, Conceptualization, Methodology, Investigation, Formal analysis, Software, Data Curation, Review & Editing Preparation, Writing-Original Draft, Preparation. MÖ: Statistical analyses, Visualization, Investigation, Data Curation, Conceptualization, Methodology, Formal analysis. All authors read and approved the final manuscript.

REFERENCES

Aydin M, Altintas N, Cem Mutlu L, *et al*., 2017. Asymmetric dimethylarginine contributes to airway nitric oxide deficiency in patients with COPD. Clin Respir J 11: 318-327.

Barnes PJ, 2020. Oxidative stress-based therapeutics in COPD. Redox Biol 33: 101544.

Blauvelt A, Langley RG, Gordon KB, *et al*., 2023. Next generation PDE4 inhibitors that selectively target PDE4B/D subtypes: a narrative review. Dermatol Ther 13: 3031-3042.

Can S, Çetik Yıldız S, Keskin C, *et al*., 2022. Investigation into the protective effects of *Hypericum Triquetrifolium Turra* seed against cyclophosphamide-induced testicular injury in Sprague Dawley rats. Drug Chem Toxicol 45: 1679-1686.

Cengiz M, Gür B, Sezer CV, *et al*., 2023. Alternations in interleukin-1β and nuclear factor kappa beta activity (NF-kB) in rat liver due to the co-exposure of Cadmium and Arsenic: Protective role of curcumin. Environ Toxicol Pharmacol 102: 104218.

Crocetti L, Floresta G, Cilibrizzi A, Giovannoni MP, 2022. An Overview of PDE4 Inhibitors in Clinical Trials: 2010 to Early 2022. Molecules 27.

Donato M, and Tolosa L, 2021. High-Content Screening for the Detection of Drug-Induced Oxidative Stress in Liver Cells. Antioxidants (Basel) 10.

Fan T, Wang W, Wang Y, *et al*., 2024. PDE4 inhibitors: potential protective effects in inflammation and vascular diseases. Front Pharmacol 15: 1407871.

Flemming S, Schlegel N, Wunder C, *et al*., 2014. Phosphodiesterase 4 inhibition dose dependently stabilizes microvascular barrier functions and microcirculation in a rodent model of polymicrobial sepsis. Shock (Augusta, Ga) 41: 537-545.

Gezer A, and Karadağ SE, 2023. Investigation of apoptotic and autophagic effects of chronic roflumilast use on testicular tissue in rats by immunohistochemical and immunofluorescence methods. Iran J Basic Med Sci 26: 276-284.

Gür F, Ağgül AG, and Gülaboğlu M, 2020. Su ile hazırlanan zeytin yaprağı özütünün ratlarda streptozotosin kaynaklı oksidatif stres ve lipit peroksidasyonu üzerine etkileri. J Ins Sci Technol 10: 2406-2415.

Gür F, Cengiz M, Gür B, *et al*., 2023. Therapeutic role of boron on acrylamide-induced nephrotoxicity, cardiotoxicity, neurotoxicity, and testicular toxicity in rats: Effects on Nrf2/Keap-1 signaling pathway and oxidative stress. J Trace Elemen Med Biol 80: 127274.

He Y, Huang Y, Mai C, *et al*., 2020. The immunomodulatory role of PDEs inhibitors in immune cells: Therapeutic implication in rheumatoid arthritis. Pharmacol Res 161: 105134.

Ismail M, Hossain MF, Tanu AR, Shekhar HU, 2015. Effect of spirulina intervention on oxidative stress, antioxidant status, and lipid profile in chronic obstructive pulmonary disease patients. Biomed Res Int 486120.

Janjua S, Fortescue R, and Poole P, 2020. Phosphodiesterase-4 inhibitors for chronic obstructive pulmonary disease. Cochrane Database Syst Rev 5.

Ju J, Li Z, and Shi Q, 2022. Baicalin Inhibits Inflammation in Rats with Chronic Obstructive Pulmonary Disease by the TLR2/MYD88/NF-κBp65 Signaling Pathway. Evid Based Complement Alternat Med 7273387.

Kim SY, An TJ, Rhee CK, *et al*., 2021. The effect and associated mechanism of action of phosphodiesterase 4 (PDE4) inhibitor on CD4+ lymphocyte proliferation. Clin Exp Pharmacol Physiol 48: 221-226.

Lewis SM, Williams A, and Eisenbarth SC, 2019. Structure and function of the immune system in the spleen. Sci Immunol 4.

Liu X, Zhang H, Wang Y, *et al*., 2020. Fractional Exhaled Nitric Oxide is Associated with the Severity of Stable COPD. Copd: Chronic Obstr Pulm Dis 17:(2), 121-127.

Luo W, Long Y, Feng Z, *et al*., 2021. A γ-glutamylcysteine ligase AcGCL alleviates cadmium-inhibited fructooligosaccharides metabolism by modulating glutathione level in Allium cepa L. J Hazard Mater 419: 126255.

Montrose D, and Galluzzi L, 2019. Cellular Nutrient Utilization and Cancer. In: Sulfur metabolism and its contrubition to malignancy. Academic Press. San Diego, USA, 39-83.

Nguyen HO, Tiberio L, Facchinetti F, *et al*., 2023. Modulation of human dendritic cell functions by phosphodiesterase-4 inhibitors: potential relevance for the treatment of respiratory diseases. Pharmaceutics 15: 2254.

Phillips JE, 2020. Inhaled phosphodiesterase 4 (PDE4) inhibitors for inflammatory respiratory diseases. Front Pharmacol 11: 259.

Sahin B, Karabulut S, Filiz AK, *et al*., 2022. Galium aparine L. protects against acetaminophen-induced hepatotoxicity in rats. Chem Biol Interact 366: 110119.

Strong VD, 2014. Molecular correlates of multiday memory in an appetitive conditioning model: insights into mediators of memory extension. PhD Thesis. Memorial University of Newfoundland.

Szczypka M, 2020. Role of phosphodiesterase 7 (PDE7) in T cell activity. Effects of selective PDE7 inhibitors and dual PDE4/7 inhibitors on T cell functions. Int J Mol Sci 21: 6118.

Xu J, Luo Y, Yuan C, *et al*., 2020. Downregulation of nitric oxide collaborated with radiotherapy to promote anti-tumor immune response via inducing CD8+ T cell infiltration. Inter J Biol Sci 16: 1563.

Yang Y, Lenherr ED, Gromes R, *et al*., 2019. Plant glutathione biosynthesis revisited: redox-mediated activation of glutamylcysteine ligase does not require homo-dimerization. Biochem J 476: 1191-1203.

Zhang C, Zhu W, Meng Q, *et al*., 2022. Halotherapy relieves chronic obstructive pulmonary disease by alleviating NLRP3 inflammasome-mediated pyroptosis. Ann Transl Med 10: 1279.